Review of the Development and Testing of a New Family of Boron and Gadolinium-Bearing Dual Thermal Neutron Absorbing Alloys – 13026

M. L. Schmidt 1*, G. J. Del Corso 2*, K. A. Klankowski 3*, L. W. Lherbier 4** and D. J. Novotnak 5**
* Carpenter Tech., Corp., P.O. Box 14662, Reading PA 19612-4662; mschmidt@cartech.com
** Carpenter Powder Products, 600 Mayer St., Bridgeville, PA 15017; llherbier@cartech.com

ABSTRACT

The development of a new class of Fe-based thermal neutron absorbing alloys (patent pending) containing both natural boron (B) and gadolinium (Gd) is reviewed. Testing has shown that Ar and N inert gas atomized powder metallurgy (PM) variants offer superior processability coupled with improved mechanical properties that exhibit reduced anisotropy and reduced corrosion rates compared to conventional cast/wrought processed material. PM processing results in a microstructure containing a uniform distribution of second phase borides and gadolinides, and the morphology of the gadolinides prevents the formation low melting point Gd-bearing phases at solidifying austenite boundaries. The new T316-based materials containing both B and Gd exhibit superior corrosion resistance compared to straight B-bearing T304 materials. By keeping the B content < 1 weight percent (%) and using Gd to attain an equivalent B (B_{Eq}) content higher than that achievable through the use of B only, the new materials exhibit superior ductility, toughness and bendability as a result of significantly reduced area fraction of Cr-rich M_2B borides. Limiting the total area fraction of second phase particles to < 22% insures a product with superior bendability. By restricting B to < 1% and using Gd up to 2.5%, B_{Eq} levels approaching 12% can be attained that provide a cost effective improvement in thermal neutron absorption capability compared to using B-10 enriched boron. The new materials can be easily bent during fabrication compared to existing metal matrix composite materials while offering similar thermal neutron absorption capability. Production lots containing B_{Eq} levels of 4.0 and 7.5% (Micro-Melt® DuoSorb™ 316NU-40 and 75, respectively) are in the process of being fabricated for customer trial material.

INTRODUCTION

Boron is the traditional standard thermal neutron absorber for containment of spent nuclear fuel materials. It has the sixth largest thermal neutron cross-section of all naturally occurring materials; however, its low atomic mass makes it the second most effective alloying addition on a weight percent basis. Much of the thermal neutron absorption capabilities of boron are derived from the B-10 isotope [1], however B-10 enriched boron is generally cost prohibitive for use in commercial alloy systems, and as such natural boron (B), which typically contains 18.4 weight percent (%) B-10, is used. Boron has little or no solubility in stainless steel or nickel-based alloys, instead it generally forms borides that are enriched with Cr, Mo and Fe.[2] For example, in Carpenter Technology Corporation's Micro-Melt® NeutroSorb® alloy system a Cr-rich M_2B phase forms with a composition of 46% Cr, 40% Fe, 3.5% Mn, 1.0% Ni and 9.5% B.[3]

There has been much interest in replacing boron with gadolinium (Gd) in thermal neutron absorption alloys. Gadolinium is a lanthanoid, and has the highest thermal neutron cross-section by a considerable margin. Despite its high atomic mass, Gd safely remains the most efficient thermal neutron absorbing

alloy addition, needing only approximately 0.23% (based on the atomic mass and natural thermal neutron absorption cross-section (barns) differences between B and Gd) to supply the equivalent thermal neutron absorption characteristics as 1.0% B. Like B, Gd has little or no solubility in the matrix of stainless steel or nickel-based alloys. Instead, it commonly forms Gd-rich precipitates (i.e., gadolinides) that are typically enriched with Ni, and Fe, and unlike borides, they do not deplete the matrix of Cr.[4, 5] Like B, higher Gd concentrations increase thermal neutron absorption capability and strength at the expense of ductility and toughness. In addition, intermetallic Gd phases in Fe-based alloy systems can lead to hot-workability issues due to their low liquation temperature and extended melting temperatures.[6] The use of Gd to enhance a material's thermal neutron absorption capabilities can offer a cost advantage compared to enrichment with B-10 when the previously referenced processability issues can be overcome.

Carpenter Technology Corp. has historically supplied Micro-Melt® NeutroSorb®, a series of T304-based borated stainless steel alloys containing 0.45 to 2.25% B (ASTM A887-89) that are manufactured using powder metallurgy (PM) technology for the spent nuclear fuel storage industry. These materials have been used primarily in the fabrication of spent fuel storage racks, cask baskets, control rods, burnable poison and shielding. Based on customer input requesting a material with improved processability, corrosion resistance and higher thermal neutron absorption capability than T304B7 borated stainless steel, the highest boron containing alloy in ASTM A887-89 (i.e., 1.74 – 2.25% B), Carpenter has developed a new family of processable T304 and T316-based stainless steel alloys that use both B and Gd to absorb thermal neutrons.

DESCRIPTIONS AND DISCUSSIONS

Conventional Cast/Wrought Versus PM Processed Material

TABLE I. Heat Chemistries of Comparable Cast/Wrought (VIM) and PM Austenitic Materials Containing B and Gd

	Composition (w/o)									
	Alloy #1		Alloy #2		Alloy #3		Alloy #4		Alloy #5	
Element	VIM 002046	PM 130881	VIM 002047	PM 130866	VIM 002048	PM 130869	VIM 002049	PM 130870	VIM 002050	PM 130868
Mn	0.31	0.39	0.83	0.89	1.14	1.18	1.20	1.22	1.14	1.16
Si	0.20	0.20	0.23	0.24	0.34	0.27	0.38	0.40	0.33	0.34
Cr	22.12	22.12	18.12	18.16	20.22	20.44	20.66	20.76	20.34	20.52
Ni	18.56	18.25	10.35	10.16	11.62	11.73	11.64	1.64	15.14	15.16
Mo	2.78	2.88	4.13	4.22	0.06	0.11	<0.01	<0.01	4.05	4.13
Gd	0.42	0.44	0.32	0.27	0.79	0.66	0.46	0.54	0.33	0.26
B	0.39	0.40	0.12	0.26	0.62	0.62	1.10	1.14	0.54	0.58

The alloys shown in Table I were prepared by VIM casting 101.60 mm square x 18.14 kg ingots (heats 002046 – 002050) or by Ar atomization (heats 130881, 130866, 130869, 130870 and 130868), screening to -40 mesh and hot isostatically pressing (HIP) into 114.30 mm square x 18.40 kg compacts from 1121°C. All material was processed to 19.10 mm thick hot-rolled plate where possible. Alloys 1 and 2

were hot-worked/rolled from 1050°C and annealed at 1050°C for 3600s and quenched into water, while alloys 3 through 5 were hot-worked/rolled from 1000°C and annealed at 1100°C.

a. Cast/wrought material b. PM material

Fig. 1. Representative images of 19.10 mm hot-rolled annealed plate of the materials in Table I.

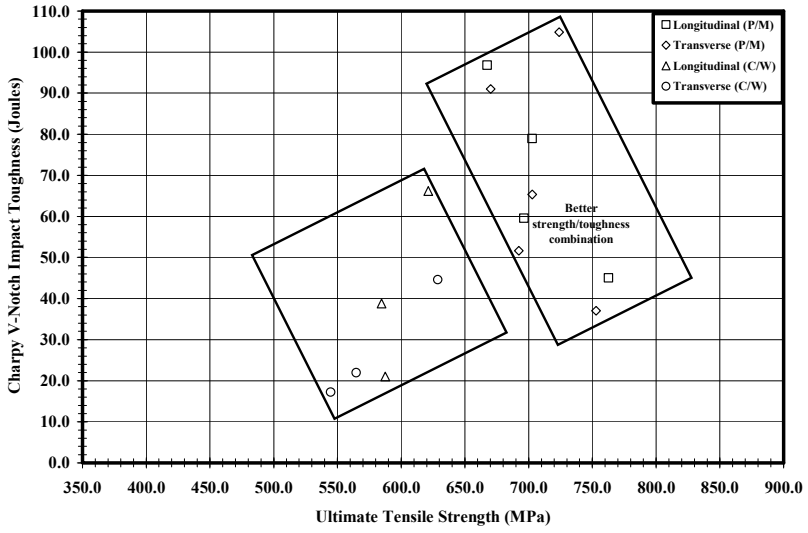

Fig. 2. CVN impact toughness versus UTS test results for the materials in Table I.

All of the cast wrought alloys, except for heat 002047, which was balanced to provide a duplex structure, developed hot-tears during press forge conversion to billet that became enhanced with further processing to plate (Figure 1a), while none of the PM processed alloys displayed this condition (Figure 1b). The phase balance of 002047 was adjusted based on Ziolkowski's work [7], which showed that the workability of austenitic material containing 0.76 – 1.09% Gd could be improved if the alloy (T304/T305 and T321/T347 austenitic stainless steel) is rebalanced to preferentially contain 10 – 15% ferrite. The ferritic phase results in the formation of a discontinuous Gd intermetallic phase while the austenitic phase results in the formation of a continuous Gd phase that had an adverse effect on hot-workability. The processing issues with 002049 and 002050 were so severe that mechanical test specimens could not be evaluated. Standard longitudinal and transverse smooth tensile specimens with a gage diameter of 6.4

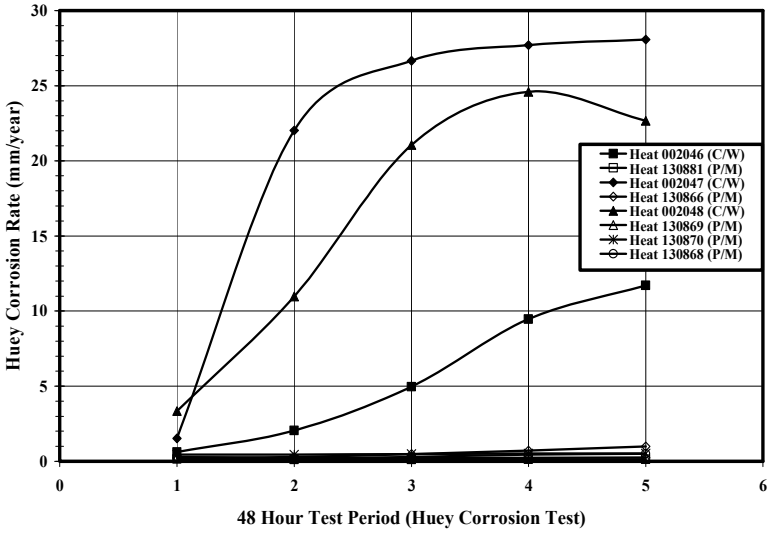

Fig. 3. Huey corrosion test results for the materials in Table I.

mm were removed, prepared and tested in triplicate at room temperature per ASTM E8, and standard Charpy V-notch (CVN) impact specimens were removed from the L-S (longitudinal) and T-L (transverse) orientations (per ASTM E399), prepared and tested in triplicate at room temperature per ASTM E-23. In addition, standard Huey corrosion coupons were removed, prepared and tested in triplicate in boiling 65 volume percent (v/o) HNO_3 for five 172,800s (48 hour, which will be used for graphing purposes) time periods per the requirements of ASTM A262-C. The results of this testing showed that the PM processed material exhibits a superior combination of CVN toughness and strength with reduced anisotropy (Figure 2) and superior Huey corrosion resistance (Figure 3). In addition, even though heat 002047 was processable, this alloy displayed the poorest corrosion resistance, as measured by the Huey test, of the evaluated cast/wrought materials due to the ferritic component in its microstructure. Thus, these findings indicate that PM processing can be used to overcome the hot workability issues associated with low melting point Gd-bearing phases that form on austenite phase boundaries during solidification of conventional cast/wrought processed alloys. As a result of this testing all future efforts were focused on the development of a PM alloy containing both B and Gd to absorb thermal neutrons.

Mechanical Property, Corrosion and Microstructural Features of the New Alloy Family

The alloys shown in Table II were prepared by Ar atomization (with the exception of heats 130878 and 130879, which were N atomized), were screened to -40 mesh and were HIP'd into 38.10 mm x 133.35 mm x 660.40 mm compacts from 1121°C. All material was hot-rolled to 19.10 mm thick plate from 1121°C and annealed at 1066°C for 3600s followed by water quenching to room temperature. In addition to the elements shown in Table II, all materials exhibited $\leq$ 0.046% C, $\leq$ 0.01% P, $\leq$ 0.005% S, $\leq$ 0.01% Cu and $\leq$ 0.02% Co. The term B_{Eq} also appears in Table II. The term B_{Eq} (Eq. 1) is a means of expressing the equivalent amount of B that would be required to account for the Gd present in the alloy and it is very useful to show compositional effects on properties and microstructure. It is derived using the relative atomic mass and the natural thermal neutron absorption cross-section (barns) equivalency of

B and Gd.

$$B_{Eq} = \%B + 4.35(\%Gd) \qquad (1)$$

Following hot-rolling and annealing, test specimen blanks were removed, processed and tested. Testing included triplicate longitudinal and long transverse room temperature smooth tensile and CVN impact toughness (L-S and L-T orientations per ASTM E399) conducted per ASTM E-8 and E-23, triplicate Huey corrosion in boiling 65 v/o HNO_3 for five 172,800s (48 hour, which was used for graphing purposes) time periods per the requirements of ASTM A262-C and triplicate bend angle testing. Each hot-rolled and annealed alloy was sectioned along its long axis to yield three blanks that were subsequently fabricated into standard Strauss bend specimens. Bend tests were performed using a 9.53 mm mandrel that bent the sample through a 39.69 mm slot with a 8.27 MPa hydraulic ram. Upon completion of the testing the bend angle was measured in degrees. While the bend test is not a standard ASTM test, it does provide a measure of fabricability, specifically with respect to the ability to bend material during the fabrication of spent fuel channels and storage racks.

TABLE II. Chemistries of the Heats Produced and Tested During the Development of the New Family of Processable PM Austenitic Stainless Steels Containing B and Gd

	Composition (w/o)									
Heat No.	**Mn**	**Si**	**Cr**	**Ni**	**Mo**	**N**	**O**	**B**	**Gd**	**B_{Eq}**
130708	1.68	0.54	19.48	13.52	<0.01	<0.001	0.004	2.06	<0.01	2.06
130709	1.71	0.52	22.05	13.58	<0.01	<0.001	0.010	2.60	<0.01	2.60
130710	1.73	0.48	24.36	13.66	<0.01	0.001	0.010	3.03	<0.01	3.03
130711	1.75	0.48	26.27	13.68	<0.10	0.001	0.010	3.51	<0.01	3.51
130712	1.71	0.52	24.01	13.44	4.42	0.001	0.009	1.50	<0.01	1.50
130713	1.76	0.48	24.12	13.53	3.89	0.001	0.011	2.98	<0.01	2.98
130715	1.99	0.53	22.12	13.50	4.04	0.001	0.013	1.14	0.06	1.40
130754	2.09	0.48	21.28	13.48	4.00	0.001	0.016	1.12	<0.01	1.12
130755	2.44	0.39	24.71	11.93	5.28	0.001	0.013	1.97	<0.10	1.97
130757	2.26	0.38	22.70	12.92	4.54	0.001	0.022	1.52	0.18	2.30
130758	2.12	0.44	21.20	13.64	3.98	0.001	0.019	1.82	0.26	2.95
130760	2.12	0.44	21.18	13.64	3.98	<0.001	0.016	1.14	0.22	2.10
130761	2.38	0.38	24.39	12.29	5.24	<0.001	0.015	2.01	0.56	4.45
130762	2.39	0.36	24.10	12.65	5.19	<0.001	0.013	2.03	1.20	7.25
130880	2.00	0.56	17.95	13.19	2.87	0.002	0.012	0.28	0.17	1.02
160105-1	2.12	0.52	20.07	13.18	3.70	0.002	0.024	1.02	1.68	8.33
130873	2.22	0.50	20.07	12.91	3.85	0.002	0.015	1.04	1.68	8.35
130874	2.55	0.44	23.51	11.62	5.11	0.002	0.013	1.98	1.80	9.81
130875	2.53	0.43	23.51	11.92	5.17	0.002	0.024	2.02	2.52	12.98
130876	2.66	0.41	25.33	11.32	5.74	0.002	0.014	2.48	2.52	13.44
130877	2.13	0.59	18.30	14.03	3.26	0.002	0.016	0.69	2.56	11.83
130878	2.03	0.55	17.82	13.17	2.87	0.162	0.016	0.23	0.13	0.80
130879	2.22	0.49	20.00	12.83	3.86	0.075	0.038	0.97	1.45	7.28

A longitudinal, mid-radius section was prepared for metallographic examination for each material. The prepared and unetched metallographic specimens were examined using scanning electron microscopy (SEM) and 10 random fields per sample were recorded. The images were recorded using the backscatter electron (BSE) detector at a magnification of 2,000X. The BSE detector was used in order to obtain atomic number contrast imaging so the Cr-rich borides, the Mo-rich borides and the Gd-rich gadolinides could be readily distinguished from one another without the need for selective etching to provide phase contrast. In addition, since the gadolinide phase(s) tend to be acid soluble, this process preserved the integrity of these phases for quantitative image analysis. All SEM/BSE images were imported into a Clemex Vision PE (version 3.5.011) image analysis system and analyzed to obtain second phase particle area fraction data. The longitudinal mechanical properties, Huey corrosion (with the rate obtained from each of the 5 test periods averaged to yield an overall corrosion rate) and bend tests results were analyzed as a function of B_{Eq}. In addition, the longitudinal mechanical properties and bend test results were analyzed as a function of the mean area fraction of the combined second phase particles (i.e., Cr-rich borides, Mo-rich borides and gadolinides).

All heats, with the exception of 130876 (B = 2.48%, Gd = 2.52% and B_{Eq} = 13.44%), were converted to 19.10 mm thick plate without any issues. Heat 130876 displayed some hot-tears/checks, which did not appear to be a result of incipient melting; rather they seemed to be associated with excessive stiffness of the material. This behavior is likely a result of the high volume fraction of boride and gadolinide second phase particles present in the structure. Indeed, quantitative image analysis revealed that this material contained area fractions of 20.69%, 5.62% and 5.54% for the Cr-rich boride, Mo-rich boride and gadolinide second phase particles, respectively. Heat 130875 (2.02% B, 2.52% Gd and 12.98% B_{Eq}) thus represents the upper limit of processability for this new alloy family.

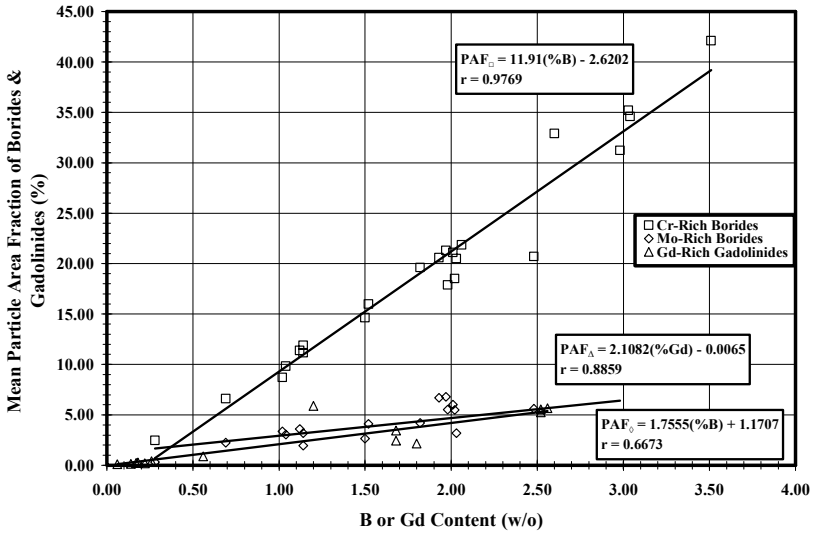

Fig. 4. Plot of mean particle area fraction versus B or Gd content for the materials in Table II.

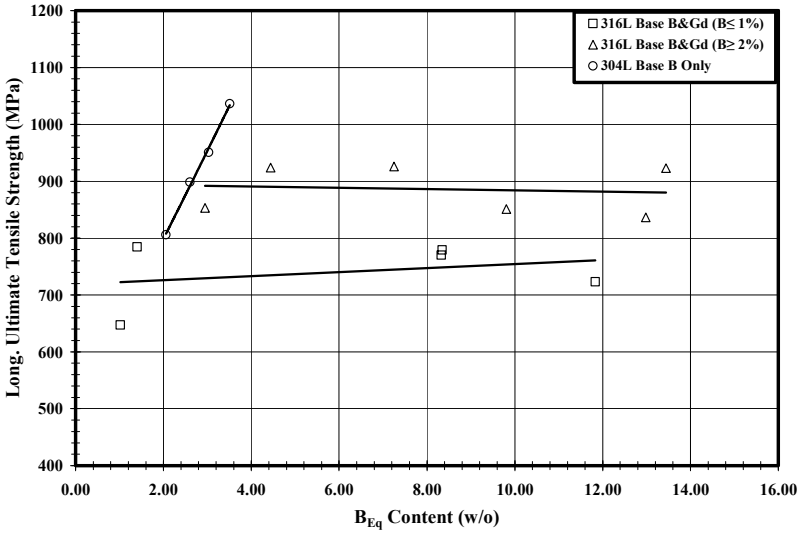

Fig. 5. Plot of longitudinal UTS versus B_{Eq} content for the materials in Table II.

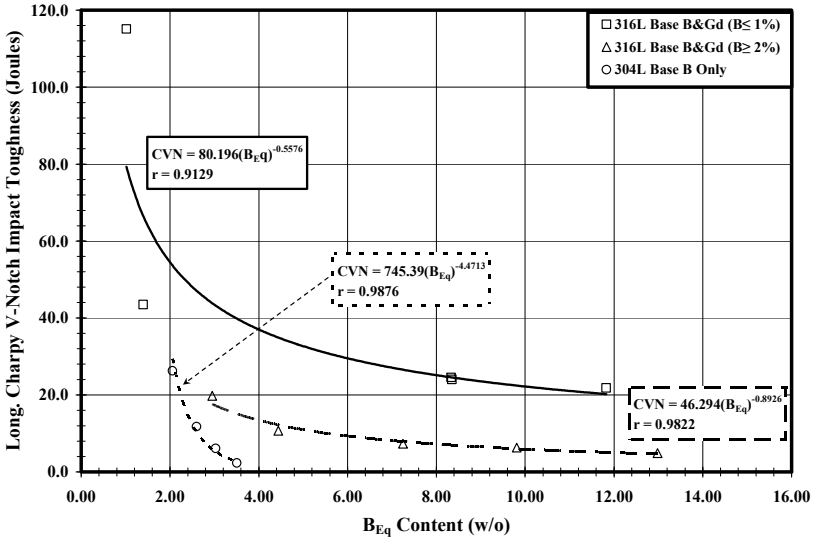

Fig. 6. Plot of longitudinal (L-T orientation) CVN impact toughness versus B_{Eq} content for the materials in Table II.

Positive linear dependency is observed for both the 0.2% YS and UTS when plotted as a function of B_{Eq}, with the heats containing B $\leq$ 1% exhibiting lower strength values for the same B_{Eq} compared to heats containing $\geq$ 2% B. In addition, the strength of straight B-bearing T304 increases at a more rapid rate over the evaluated range of B (i.e., 2.06 – 3.51%) since only Cr-rich borides are being formed and a greater area fraction of Cr-rich borides forms compared to Mo-rich borides and gadolinides for equivalent amounts of B and Gd (Figure 4). The behavior observed for the longitudinal UTS data is shown in Figure

5. In terms of ductility and toughness, a very strong, inverse dependency is exhibited by % El., % R.A. and CVN impact toughness as a function of B_{Eq} content with the heats containing $B \leq 1\%$ exhibiting superior behavior compared to heats containing $B \geq 2\%$ and the T304 heats containing B only at a comparable B_{Eq}. The CVN impact toughness behavior is best described using power curve fits of the form $Y = bX^{-m}$ as shown by the plot of longitudinal CVN impact toughness versus B_{Eq} content in Figure 6. Similar behavior was observed for the tensile ductility data, but is not shown in this paper.

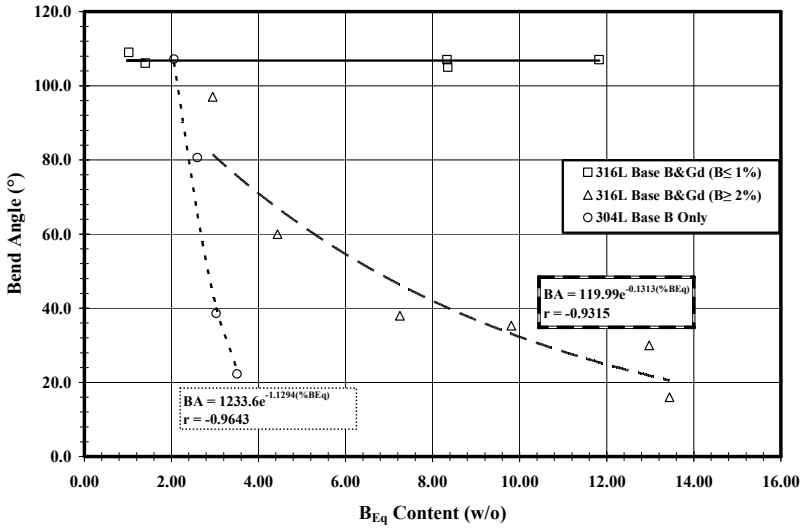

Fig. 7. Plot of bend angle versus B_{Eq} content for the materials in Table II.

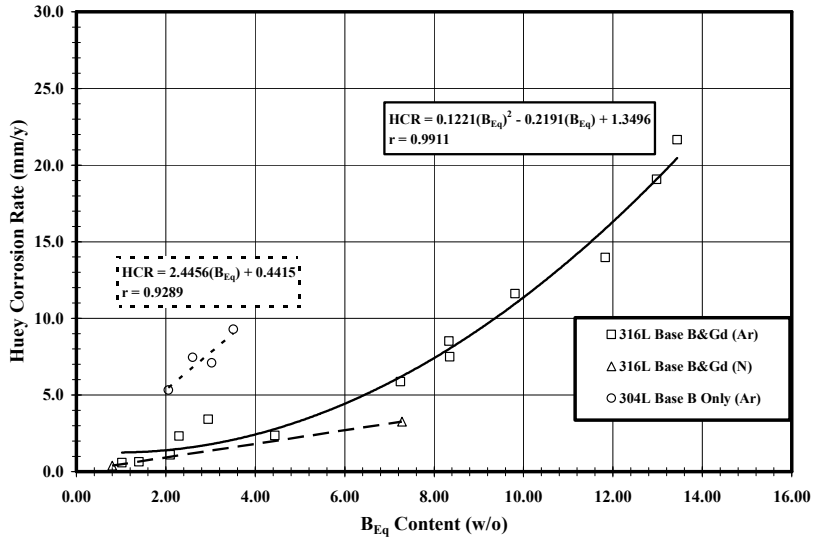

Fig. 8. Plot of Huey corrosion rate versus B_{Eq} content for the materials in Table II.

Bendability is another measure of ductility, and it is important from a fabrication viewpoint, since it provides a means to quantify the extent to which material can be bent during the fabrication of a component used to store spent nuclear fuel. Thus, the higher the bend angle, the more fabricate able the alloy/material is. The data plot of bend angle versus B_{Eq} (Figure 7) shows that heats containing B $\leq$ 1% exhibited superior bending behavior at a comparable B_{Eq} compared to material containing B $\geq$ 2% or the straight B-bearing T304 heats. Thus, these data clearly show that superior ductility, toughness and fabricability can be obtained at a comparable B_{Eq} when the B content is restricted to $\leq$ 1%. In terms of Huey corrosion rate, superior corrosion resistance of the T316-based materials containing B and Gd is exhibited when compared to the T304 B only heats (Figure 8), and there is a slight benefit in corrosion resistance for the two N atomized heats (i.e., 130878 and 130879) compared to their Ar atomized counterparts. This behavior is related to the known beneficial effect that N has on the pitting resistance equivalent number of austenitic stainless steels.

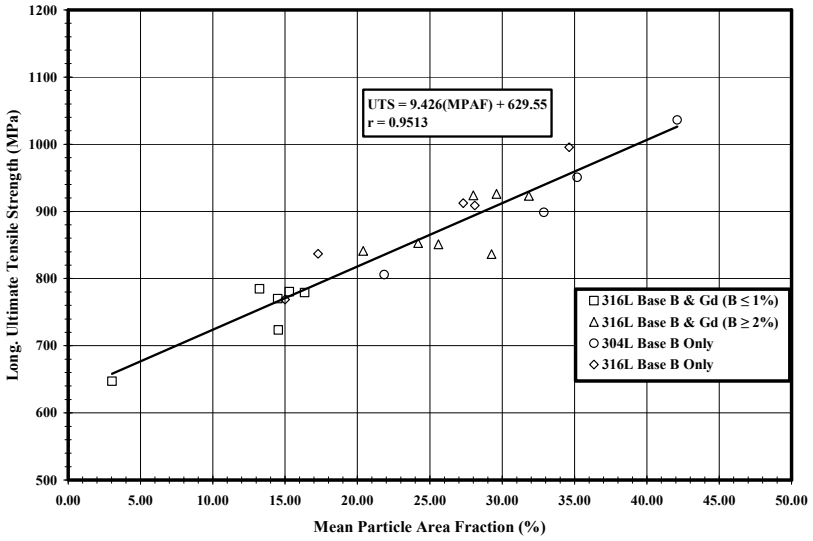

Fig. 9. Plot of longitudinal UTS versus mean particle area fraction for the materials in Table II.

The effect of microstructure on material performance is evident when mechanical test and bend angle data are examined as a function of the combined mean particle area fraction of the second phase particles. The UTS data show a strong positive, linear dependency on mean particle area fraction (Figure 9), while the tensile ductility and CVN toughness show a strong, inverse dependency on mean particle area fraction. The data fits used to describe this behavior were an exponential relationship ($Y = be^{-Xm}$) for CVN impact toughness (Figure 10) and a second order polynomial for the tensile ductility data, which are not shown in this paper. Bend angle (Figure 11) shows a rapid drop off for mean particle area fractions greater than approximately 22%. This is a further indication that the B content should be maintained at a level $\leq$ 1% to limit the formation of Cr-rich borides in order to insure good fabrication capability by end users.

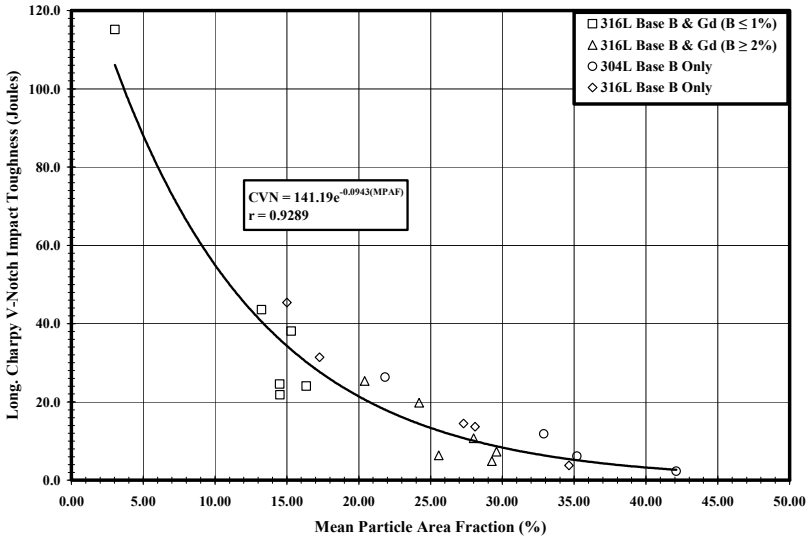

Fig. 10. Plot of longitudinal (L-S orientation) CVN impact toughness versus mean particle area fraction for the materials in Table II.

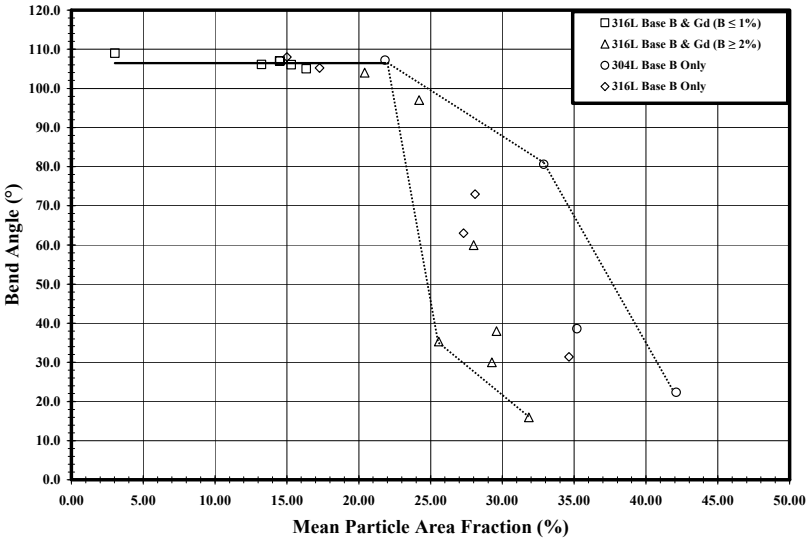

Fig. 11. Plot of bend angle versus mean particle area fraction for the materials in Table II.

Thermal Neutron Absorption Work

Five alloys of the new B and Gd-bearing T316 material, spanning a B_{Eq} of 1.02 to 11.83%, and four compositions of T304 Micro-Melt® NeutroSorb® (Table III) were evaluated to test their thermal neutron absorption efficiency. For the T304 material heats 173554, 182200, 173375 and 172678 represent ASTM

TABLE III. Chemistries of the Materials Evaluated by NETCO Using the Pennsylvania State University's Breazeale Research Reactor

	Composition (w/o) by Heat Number								
Element	**130880**	**130760**	**130879**	**160105-1**	**130877**	**173554**	**182200**	**173375**	**172678**
C	0.008	0.024	0.015	0.022	0.015	0.01	0.032	0.03	0.05
Mn	2.00	2.12	2.22	2.12	2.13	1.80	1.70	1.69	1.66
Si	0.56	0.44	0.49	0.52	0.59	0.51	0.54	0.60	0.62
P	<0.005	0.004	<0.005	0.003	<0.005	0.007	<0.005	0.007	0.019
S	0.001	0.001	0.005	0.002	0.003	0.001	0.0032	0.002	0.003
Cr	17.95	21.18	20.00	20.07	18.30	19.70	19.46	19.45	19.66
Ni	13.19	13.64	12.83	13.18	14.03	13.50	13.68	13.56	13.26
Mo	2.87	3.98	3.86	3.70	3.26	0.01	<0.10	<0.01	0.02
Cu	<0.01	<0.01	<0.01	<0.01	<0.01	0.01	0.07	<0.01	0.02
Co	<0.01	<0.01	<0.01	<0.01	<0.01	0.01	0.07	0.04	0.04
O	0.012	0.016	0.038	0.024	0.016	0.02	NR	0.010	0.022
Gd	0.17	0.22	1.45	1.68	2.56	0.00	0.00	0.00	0.00
N	0.002	<0.001	0.075	0.002	0.002	0.05	0.008	0.063	0.052
B	0.28	1.14	0.97	1.02	0.69	1.06	1.46	1.58	1.88
B_{Eq}	1.02	2.10	7.28	8.33	11.83	1.06	6.07	1.58	1.88

TABLE IV. Results of the Testing Performed on Representative Heats of the New B and Gd Thermal Neutron Absorbing Alloy and Heats of Standard Micro-Melt® NeutroSorb® Alloy Using the Pennsylvania State University's Breazeale Research Reactor and NETCO

	Composition (w/o)			Results from Breazeale Reactor Testing			
Heat #	**B-10**	**Gd-155,157**	**B-10 + Gd-155,157**	**Counts**	**Count Time (sec.)**	**Counts/Sec.**	**Corrected Transmitted Ratio (%)**
Incident	N/A	N/A	N/A	13,152,071	300	43,840.2	100.00
130880	0.05	0.05	0.10	594,561	30	19,818.7	45.08
130760	0.21	0.07	0.28	341,188	30	11,372.9	25.86
130879	0.18	0.44	0.62	85,066	30	2,835.5	6.39
160105-1	0.19	0.51	0.70	74,953	30	2,498.4	5.60
130877	0.13	0.77	0.90	51,115	30	1,703.8	3.75
173554	0.20	0.00	0.20	528,701	30	17,623.4	40.74
182200	1.12	0.00	1.12	43,185	30	1,439.5	3.16
173375	0.29	0.00	0.29	399,161	30	13,305.4	30.34
172768	0.35	0.00	0.35	309,169	30	10,305.6	23.73

A877 T304B4, T304B5, T304B6 and T304B7, respectively, with heat 182200 containing 0.42% natural B and 1.04% B-10. Single test coupons measuring 50.80 mm x 101.60 mm x 2.54 mm thick were prepared from each of the annealed materials in Table III. These samples were used for thermal neutron absorption testing at the Pennsylvania State University's Neutron Beam Laboratory located at the

Breazeale research reactor. This work was contracted to North East Technology Company (NETCO) and was performed on-site on April 17, 2012. The testing was conducted in accordance with NETCO special engineering procedure SEP-300039-01, and all test data were collected and reported under the provisions of NETCO's compliant quality assurance program (10CFR50 Appendix B and 10CFR21). Transmission ratio test data (defined as the corrected count rate of the sample over the corrected count rate of the incident beam) were reported for the nine test specimens as well as NETCO standard materials representing BORAL® (a registered trademark to Ceradyne, Inc), Metamic™ (Metamic, LLC trademark) and hot pressed B_4C.[8] The thermal neutron transmission ratio (TNTR) data from the testing of the five lots of B and Gd-bearing T316-based and the four lots of B-bearing T304-based materials were analyzed as a function of isotopic B-10 + Gd-155,157 content. Data from the NETCO standards along with select data from the Carpenter supplied material were analyzed as a function of sample thickness.

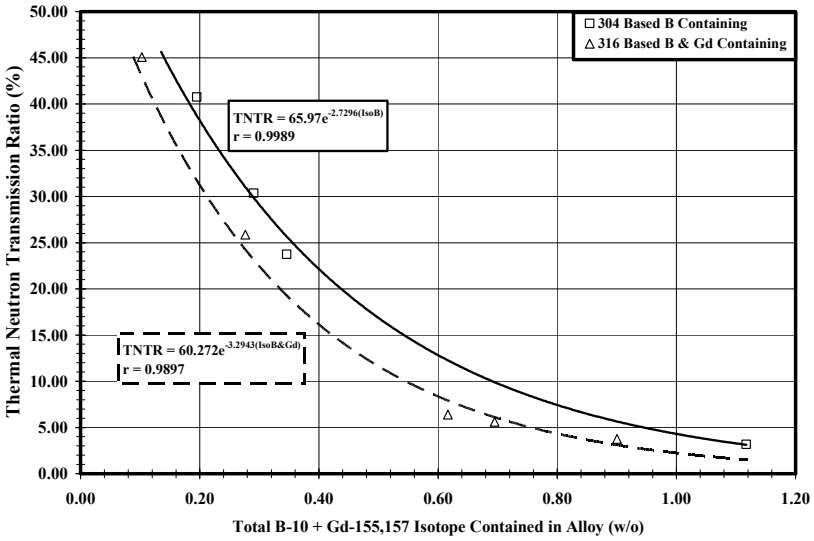

Fig. 12. Plot of thermal neutron transmission ratio versus total B-10 + Gd-155,157 isotopic content for the materials in Table III and the data in Table IV.

The results of the testing performed on the five lots of B and Gd-bearing T316-based material and the four lots of B-bearing T304-based material by NETCO (Table IV) are plotted as a function of the total isotopic B-10 + Gd-155,157 content (Figure 12) and show very strong inverse non-linear relationships of the general form TNTR = b(B-10 + Gd-155,157 content)$^{-M}$. The plots in Figure 12 show that heat 130877 (0.69% B and 2.56% Gd) provides a comparable TNTR to heat 182200, which was enriched with 1.04% B-10 isotope. Based on the current market prices of Gd (≈ $660/kg) and B-10 (≈ $11,000/kg), heat 130877 attains this TNTR in a more cost effective manner than heat 182200. Figure 12 also shows that the TNTR associated with heats 130879 and 160105-1 approach 5%, which is more than sufficient for most applications, and far superior to that attained by the existing commercially available alloys represented by heats 173554 (T304B4), 173375 (T304B6) and 172768 (T304B7).

TABLE V. Results of the Comparative Testing Performed on NETCO's Pressed B_4C, Boral® and Metamic™ Standards Using the Pennsylvania State University's Breazeale Research Reactor

Background Information				Results from Breazeale Reactor Testing			
Material	**I.D.**	**% B**	**Thickness (mm)**	**Counts**	**Count Time (sec.)**	**Counts/sec.**	**Corrected Transmission Ratio (%)**
Pressed B_4C Standards	0.020	78.50	0.508	68,317	30	2,277.2	5.04
	0.025	79.50	0.635	43,820	30	1,460.7	3.22
	0.020	80.50	0.508	24,227	30	807.6	1.70
	0.045	81.50	1.143	19,400	90	215.6	0.33
	0.050	82.50	1.270	18,252	120	152.1	0.19
	0.055	83.50	1.397	15,063	120	125.5	0.13
Boral® Standards	PP-8	14.95	1.905	353,634	60	5,893.9	13.49
	HE-8900	19.39	2.540	96,721	60	1,612.0	3.56
	DH-7	26.52	1.905	86,187	60	1,436.5	3.15
	YK-320523	29.12	1.905	59,758	60	996.0	2.15
	TP-2104	34.46	2.540	35,098	120	292.5	0.52
Metamic® Standards	0.026	31	0.660	768,821	60	12,813.7	29.45
	0.0505	31	1.283	267,737	60	4,462.3	10.19
	0.074	31	1.880	107,742	60	1,795.7	4.00
	0.100	31	2.540	46,475	60	774.6	1.62

Figure 13 shows that the TNTR of the pressed B_4C standards and the Metamic™ standards (Table V) exhibits very strong inverse non-linear behavior as a function of specimen thickness (T). This exponential relationship is of the general form $TNTR = b \bullet e^{-M(T)}$. Figure 13 also shows the efficacy of heat 130877 (0.69% B and 2.56% Gd) compared to the B-10 enriched T304B5 material (heat 182200). In addition, the TNTR of this material is on par with 2.54 mm thick BORAL® containing 19.39% B, with 1.91 mm thick BORAL® containing 26.52% B, with 1.88 mm thick Metamic™ containing 31% B and with 0.51 and 0.64 mm thick pressed B_4C.

BORAL® is a hot-rolled composite plate material consisting of a core of mixed Al and boron carbide particles sandwiched between sheets of 1100 series Al. Metamic™ is a discontinuously reinforced Al/B_4C metal matrix composite material. Both types of products are used in the fabrication of spent fuel storage racks and contain significantly higher B contents than are achievable in the current ASTM A877 Grade A or B material. However, unlike the B-bearing T304-based material and the new B and Gd-bearing T316/304-based material, they cannot be bent or welded during fabrication, and they exhibit higher corrosion rates that precluded their use as fuel basket plates in TAD casks.[9] In addition it has been reported that the BORAL® product is prone to swelling and blistering as a result of H_2 gas evolution.[10] The data generated in this study show that the new B and Gd-bearing T316-based material can be used as a more processable, corrosion resistant alternative to both the BORAL® and Metamic™ products, and these alloys should not be prone to the swelling and blistering issues that have been reported for BORAL® products, since they represent a monolithic product.

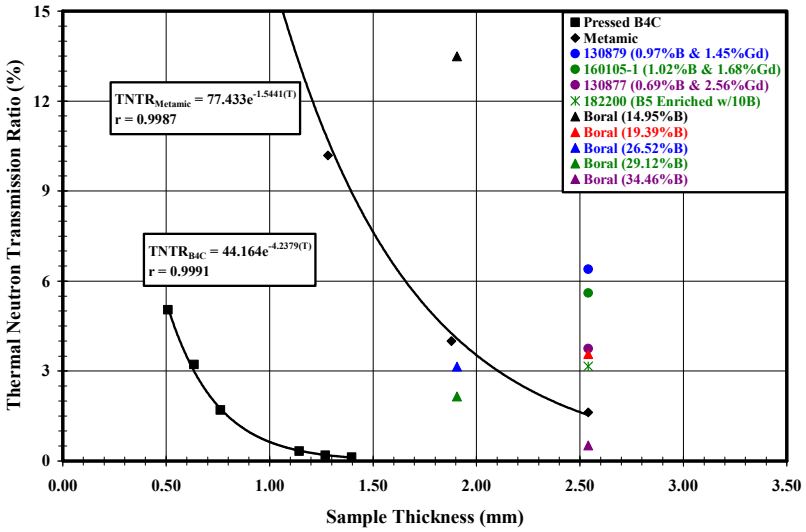

Fig. 13. Plot of thermal neutron transmission ratio versus sample thickness for the pressed B_4C, Metamic™ and BORAL® NETCO standards (Table V) along with the B and Gd-bearing 316-based and B-bearing 304-based samples (Table IV) provided by Carpenter.

CONCLUSIONS

A new family of PM processable austenitic stainless steels containing B and Gd has been developed (patent pending) based on either a T304 or a T316 composition. When produced using PM processing, these alloys exhibit a superior combination of toughness and strength coupled with reduced anisotropy and improved corrosion resistance compared to conventional cast/wrought processed material. PM processing results in a microstructure that contains a uniform distribution of second phase borides and gadolinides, and the morphology of the gadolinides is such that films of low melting point Gd-bearing phases that plague conventional cast/wrought products are avoided. The alloys can be produced using either Ar or N inert gas atomization.

The new T316-based materials containing B and Gd exhibit superior corrosion resistance compared to straight B-bearing T304 materials. By keeping the B content < 1% and using Gd to attain an equivalent B content higher than that achievable through the use of B only, the new material exhibits superior ductility, toughness and bendability. This behavior is due to a significant reduction in the area fraction of the Cr-rich boride phase (M_2B) that typically forms in T304 material containing only B. Limiting the total area fraction of second phase particles to < 22% insures a product with superior bendability.

By restricting B to < 1% and using Gd up to 2.5%, B_{Eq} levels approaching 12% can be attained that provide improved thermal neutron absorption in a cost effective manner compared to using B-10 enriched boron as a supplemental thermal neutron absorber. Compared to existing metal matrix composite materials, the new materials can be bent during fabrication and they offer similar thermal neutron absorption capability. Production lots containing B_{Eq} levels of 4.0 and 7.5% (Micro-Melt® DuoSorb™

316NU-40 and 75, respectively) are in the process of being fabricated for customer trial material.

REFERENCES

1. Solimen, S. E., D.L. Youchison, A.J. Baratta, and T.A. Balliett, "Neutron Effects on Borated Stainless Steels," Nuclear Technology, Vol. 96, pp. 346-352, December, 1991.
2. Lister, T., R. Mizia, A. Erickson, and T. Trowbridge, "Electrochemical Corrosion Testing of Neutron Absorber Materials," Idaho National Laboratory Report INL.EXT-06-11772 Rev. 1, performed under DOE contract AC07-05ID14517, May 2007.
3. Martin, J. W., "Effects of Boron Content and Processing on Mechanical Properties and Microstructure of Borated Stainless Steels," Carpenter R&D Technical Report K86007, September 23, 1988.
4. Robino, C. V., J. N. Dupont, R. E. Mizia, J. R. Michael, D. B. Williams, and E. Shaber, "Development of Gd-Enriched Alloys for Spent Nuclear Fuel Applications—Part 1. Preliminary Characterization of Small Scale Gd-Enriched Stainless Steels," Journal of Materials Engineering and Performance, Vol. 12, pp. 206-214, April, 2003.
5. DuPont, J. N., Z. Q. Liu, S. W. Banovic, and D. B. Williams, "Preliminary Microstructural Investigation of Gadolinium – Enriched Stainless Steels for Spent Nuclear Fuel Baskets," Account of work performed for the Department of Energy, August, 2000.
6. Mizia, R. E., T. E. Lister, P. J. Pinhero, and T. L. Trowbridge, "Localized Corrosion of A Neutron Absorbing Ni- Cr-Mo-Gd Alloy," Idaho National Engineering and Environmental Laboratory, April, 2005.
7. Ziolkowski, W. C., "Austenitic Stainless Steel Alloy," United States Patent 3,362,813, January 9, 1968.
8. Eyre, M. L., Letter Report on Thermal Neutron Absorption Testing Performed at Penn State University's Breazeale Reactor, May 31, 2012.
9. Van Konynenburg, R. A., P. G. Curtis and T. S. E. Summers, "Scoping Corrosion Tests on Candidate Waste Package Basket Materials for the Yucca Mountain Project," UCRL-ID-130386, Lawrence Livermore National Laboratory, Livermore, CA, March 1998.
10. Smith, R. J., G. W. Loomis and C. P. Deltete, "Borated Stainless Steel Application in Spent-Fuel Storage Racks," TR-100784, Palo Alto Ca, Electric Power Research Institute, TIC: 225730, 1992.